Energy & Environmental Science

PAPER

Edge-carboxylated graphene nanoplatelets as oxygen-rich metal-free cathodes for organic dye-sensitized solar cells†

Cite this: DOI: 10.1039/c3ee43732a

Myung Jong Ju,‡[a] In-Yup Jeon,‡[d] Kimin Lim,‡[b] Jae Cheon Kim,[c] Hyun-Jung Choi,[d] In Taek Choi,[a] Yu Kyung Eom,[a] Young Jin Kwon,[a] Jaejung Ko,*[b] Jae-Joon Lee,*[c] Jong-Beom Baek*[d] and Hwan Kyu Kim*[a]

Received 14th November 2013
Accepted 10th December 2013

DOI: 10.1039/c3ee43732a

www.rsc.org/ees

Edge-carboxylated graphene nanoplatelets (ECGnPs) were synthesized by the simple, efficient and eco-friendly ball-milling of graphite in the presence of dry ice and used as oxygen-rich metal-free counter electrodes (CEs) in organic dye-sensitized solar cells (DSSCs), for the first time. The resultant ECGnPs are soluble in many polar solvents including 2-propanol due to the polar nature of numerous carboxylic acids at edges, allowing an electrostatic spray (e-spray) to be deposited on fluorine-doped SnO_2 (FTO)/glass substrates. The ECGnP-CE exhibited profound improvements in the electrochemical stability for the $Co(bpy)_3^{2+/3+}$ redox couple compared to the platinum-CE. The charge transfer resistance (R_{CT}), related to the interface between an electrolyte and a CE, was significantly reduced to 0.87 Ω cm^2, much lower than those of platinum (Pt)-CE (2.19 Ω cm^2), PEDOT:PSS-CE (2.63 Ω cm^2) and reduced graphene oxide (rGO)-CE (1.21 Ω cm^2). The DSSC based on the JK-303-sensitizer and ECGnP-CE displayed a higher photovoltaic performance (FF, J_{sc}, and η, 74.4%, 14.07 mA cm^{-2} and 9.31%) than those with the Pt-CE (71.6%, 13.69 mA cm^{-2} and 8.67%), PEDOT:PSS (68.7%, 13.68 mA cm^{-2} and 8.25%) and rGO-CE (72.9%, 13.88 mA cm^{-2} and 8.94%).

Broader context

Dye-sensitized solar cells (DSSCs) are well-known as photovoltaic devices with low-cost and simple fabrication. However, the components of conventional DSSCs should be replaced with cheaper and eco-friendly materials for practical uses. The counter electrode (CE) is one of the most crucial components regulating the efficiency of DSSCs. Platinum (Pt) has been widely employed as the standard CE in conventional DSSCs. However, Pt is an expensive and scarce noble metal, which causes a problem for its large scale production. In the present study, edge-carboxylated graphene nanoplatelets (ECGnPs) were synthesized by the simple ball-milling of graphite with dry ice and used as oxygen-rich metal-free CEs in organic DSSCs. As a result, we demonstrate that the ECGnP on F-doped SnO_2 (FTO)/glass exhibits superior electrocatalytic performance for the $Co(bpy)_3^{2+/3+}$ redox couple to its Pt, reduced graphene oxide (rGO) and conducting polymer of PEDOT:PSS counterparts. This suggests that the ECGnPs could be a promising candidate for the metal-free CE material in DSSCs with the Co-complex redox couple.

1. Introduction

Dye-sensitized solar cells (DSSCs) developed by O'Regan and Grätzel have been widely investigated because of their potentially simple and low cost fabrication process compared to silicon-based solar cells.[1] Hitherto, the highest power conversion efficiency (PCE) reported for a DSSC is 12.3%.[2] Although the PCEs of DSSCs are lower than those of silicon-based solar cells, there is sufficient room for improvement in the efficiency of DSSCs, which relies on the performance of a DSSC's components.[3] A typical DSSC is composed of a transparent conducting oxide (TCO), dye-adsorbed TiO_2, electrolyte and a counter electrode (CE). Among them, the CE is one of the key components of a DSSC and plays a pivotal role in regulating the device performance by catalyzing the reduction of the redox couple used as a mediator to regenerate the dye after electron injection. For efficient CEs, high electrocatalytic activity for the redox couples and good electrical conductivity to transport charges are prerequisites. Platinum (Pt) has been known to best satisfy these requirements. However, Pt is an expensive and scarce noble metal, which causes a problem for its large scale production and thus limits its practical application in DSSCs.

[a]Global GET-Future Lab. & Department of Advanced Materials Chemistry, Korea University, Sejong 339-700, Korea. E-mail: hkk777@korea.ac.kr

[b]Photovoltaic Materials & Department of Advanced Materials Chemistry, Korea University, Sejong 339-700, Korea. E-mail: jko@korea.ac.kr

[c]Nanotechnology Research Center & Department of Applied Chemistry, Konkuk University, Chungju 380-701, Korea. E-mail: jjlee@kku.ac.kr

[d]Interdisciplinary School of Green Energy/Low-Dimensional Carbon Materials Center, Ulsan National Institute of Science and Technology (UNIST), Ulsan 689-798, Korea. E-mail: jbbaek@unist.ac.kr

† Electronic supplementary information (ESI) available. See DOI: 10.1039/c3ee43732a

‡ These authors contributed equally to this work.

Graphene – a single layer of two-dimensional (2D) sp^2-hybridized carbon network – has attracted a great deal of interest in the past few years owing to its unique structure and exceptional physical properties, such as high electrical and thermal conductivities, mechanical flexibility, charge transport mobility, huge specific surface area, good chemical stability, and optical transparency.[4] At present, several methods have been introduced for the synthesis of graphene and/or graphene nanoplatelets (GnPs), such as micromechanical cleavage,[5] epitaxial growth on silicon carbide wafers,[6] direct synthesis by chemical vapor deposition (CVD) on metal surfaces,[7] and chemical conversion.[8] There are many attempts to replace expensive Pt CEs as electrocatalysts, such as with carbon black,[9] carbon nanoparticles,[10] carbon nanotubes,[11] graphene nanosheets,[12] reduced graphene oxide (rGO),[13] inorganic materials,[14] and conducting polymers[15] in DSSCs. However, highly defective or defect-free graphene has been hardly suitable for the CE in DSSCs, because it is important for the graphene-based CE to simultaneously balance electrical conductivity for efficient charge transfer and high reduction activity for redox couples. Hence, heteroatom-doping (*e.g.*, N, B, O and P) into the graphitic frameworks with minimum structural damage could induce electrocatalytic active sites with a minimized change of the conjugation length.[16] Aksay *et al.*[17] reported that the catalytic activity in graphene may be due to the oxygen containing functional groups (hydroxyls, epoxides, carboxyls, and carbonyls) achieved by controlling the amount of oxygen functional groups *via* thermal annealing. In addition, we have recently demonstrated improved electrocatalytic performances of nitrogen-doped graphene nanoplatelets (NGnPs) for the $Co(bpy)_3^{2+/3+}$ redox couple.[18]

The replacement of the ubiquitous I^-/I_3^- redox couple would be a critical improvement because of its disadvantages in terms of corrosion of metal-based current collectors (especially for silver) and evaporation losses.[19] Recently, as many attempts to replace the traditional I^-/I_3^- redox couple, such as iodine-free liquid electrolyte, based on metal complexes,[20] organic,[19,21] or inorganic materials,[22] have been developed for the DSSCs. Among them, the Co-complex based DSSCs with Pt CEs exhibited a higher open circuit voltage (V_{oc}) than the I^-/I_3^- redox couple, which significantly influenced the PCE of a DSSC ($\eta \propto V_{oc} \times J_{sc} \times FF$).[23–25] For the Co-complex redox couple, however, the charge transfer resistance (R_{CT}) of Pt CEs is generally high, leading to losses in the fill factor (FF) and PCE, and their electrochemical stability is also relatively poor.[13,18]

In the present study, edge-selectively carboxylated graphene nanoplatelets (ECGnPs) were prepared by the simple ball-milling of graphite in the presence of dry ice (solid phase of carbon dioxide).[26] The resultant ECGnPs were highly dispersible in various solvents to self-exfoliation into single- and few-layer (≤5 layers) graphene nanosheets (GNs). The electrical conductivity of a thermally decarboxylated ECGnP film was as high as 1214 S cm^{-1}, which is superior to its GO counterpart.[26] Here we used the ECGnPs as oxygen-rich metal-free CEs of the organic DSSCs in conjunction with a $Co(bpy)_3^{2+/3+}$ redox couple. The difference in electronegativity between carbon ($\chi = 2.55$) and oxygen ($\chi = 3.50$) in ECGnPs should be attributed to high charge polarization for better affinity with the positively charged Co-complex redox couple, resulting in high electrocatalytic performance.

2. Experimental

Materials

Edge-selectively carboxylated graphene nanoplatelets (ECGnPs) were prepared by ball-milling graphite in the presence of dry ice followed by a modified literature procedure.[26] In brief, mechanochemically driven graphitic C–C bond dissociations in a ball-mill crusher generate active carbon species (mostly carbon-radicals and carbonions), which react with carbon dioxide to yield graphene nanoplatelets (GnPs) with edge-carboxylate groups, which are subsequently acidified by exposure to air moisture and hydrochloric acid treatment. For comparison, graphene oxide (GO) was also prepared by a modified Hummers' method[27] and it was subsequently reduced using hydrazine to produce reduced graphene oxide (rGO).[28]

Preparation of ECGnPs and rGO-based counter electrodes

Homogeneously dispersed 0.1 wt% ECGnP powders in 2-propanol solution were obtained by ultrasonication for 30 min. The resultant solution was deposited directly on fluorine-doped tin oxide (FTO)/glass (TEC-8, 6–9 Ω sq^{-1}, Pilkington) substrates using an electrostatic spray (e-spray) technique. First, the ECGnP dispersed solution in 2-propanol was loaded into a plastic syringe equipped with a 23-gauge stainless steel hypodermic needle. The needle was connected to a high voltage power supply (ESN-HV30). A voltage of ~7.7 kV was applied between a metal orifice and the conducting substrate at a distance of 10 cm. The feed rate was controlled by the syringe pump (KD Scientific Model 220) at a constant flow rate of 150 μL min^{-1}. The electric field overcomes the surface tension of the droplets, resulting in the minimization of numerous charged mists containing ECGnPs. The rGO/FTO electrode was also similarly prepared as the above method. The sample electrodes were sintered at 300 °C for 30 min under a nitrogen atmosphere prior to device fabrication. For reference, a Pt CE was prepared by deposition of *ca.* 20 μL cm^{-2} of H_2PtCl_6 solution (4 mM, 2 mg of H_2PtCl_6 in 1 mL of ethanol) and sintered at 400 °C for 15 min. The conductive poly (3,4-ethylenedioxythiophene):poly(styrenesulfonate) (PEDOT:PSS)/FTO CEs were also prepared as reference electrodes for comparison and their fabrication procedures are described in the ESI†.

Fabrication of a symmetrical dummy cell

A symmetrical sandwich dummy cell was fabricated from two identical ECGnP-, rGO-, Pt- or PEDOT:PSS-FTO sheets, which were separated by 60 μm thick Surlyn (Solaronix, Switzerland) tape as a sealant and spacer leaving a 0.6 × 0.6 cm^2 active area. The sheet edges were coated by an ultrasonic soldering system (USS-9200, MBR Electronics) to improve electrical contacts. The actual distance between electrodes was measured by a digital micrometer, and the average value was about 51 μm. The cell was filled with an electrolyte solution of 0.22 M $Co(bpy)_3(BCN_4)_2$, 0.05 M $Co(bpy)_3(BCN_4)_3$, 0.1 M $LiClO_4$, and

0.8 M 4-*tert*-butylpyridine in acetonitrile through a hole in one FTO support, which was finally closed by a Surlyn seal (Dupont). Co-complexes were prepared by a reported procedure.[25]

Fabrication of DSSCs

FTO plates were cleaned in detergent solution (Sigma-Aldrich, Mucasol), water, and ethanol using an ultrasonic bath. The FTO substrates were immersed in 40 mM aqueous $TiCl_4$ solution at 70 °C for 30 min and washed with water and ethanol. A TiO_2 colloidal paste (Dyesol, 18NR-T, particle size of 20 nm) was screen-printed onto FTO/glass and sintered at 500 °C for 30 min in air. The thickness of the transparent layer was measured using an Alpha-step 250 surface profilometer (Tencor Instruments, San Jose, CA), and a paste for the scattering layer containing 400 nm sized anatase particles (CCIC, PST-400C) was deposited by screen-printing and then dried for 1 h at 120 °C. The TiO_2 electrodes were sintered at 500 °C for 30 min. The resulting TiO_2 photoanodes were immersed in a THF–ethanol (v/v, 1/2) solution containing 0.3 mM of JK-303 dye[29] and 0.3 mM of HC-A coadsorbent (SGT-301),[30] and then kept at room temperature for 12 h. The dye adsorbed TiO_2 photoanodes were assembled with ECGnP, rGO, Pt or PEDOT:PSS CEs using a thermal adhesive film (25 μm thick Surlyn) as a spacer to produce a sandwich-type cell. A drop of the electrolyte was put on the hole at the back of the counter electrode. It was introduced into the cell *via* vacuum backfilling. The cell was placed in a small vacuum chamber to remove the inside air. Exposing it again to ambient pressure causes the electrolyte to be driven into the cell. Finally, the hole was sealed with cover glass (0.1 mm thickness) using Surlyn.

Characterization

Materials characterization. Materials were characterized by both spectroscopic and microscopic analyses. Fourier transform infrared (FT-IR) spectra were recorded on a Perkin-Elmer Spectrum 100 using KBr disks. X-ray photoelectron spectra (XPS) were recorded on a Thermo Fisher K-alpha XPS spectrometer. Raman spectra were taken with a He–Ne laser (532 nm) as the excitation source by using confocal Raman microscopy (Alpha 300S, WITec, Germany). Field emission scanning electron microscopy (FE-SEM) was performed on a FEI Nanonova 230, while high-resolution transmission electron microscopy (HR-TEM) was carried out using a JEOL JEM-2100F (Cs) microscope operating at 200 kV. The TEM specimens were prepared by dipping carbon micro-grids (Ted Pella Inc., 200 Mesh Copper Grid) into well-dispersed samples in NMP or ethanol.

Electrocatalytic activities of CEs. For the evaluation of electrocatalytic properties on the sample electrodes, all electrochemical measurements were carried out with a *VersaSTAT* 3 (Version 1.31), AMETEK connected to a potentiostat at room temperature. Electrochemical impedance spectra (EIS) on the symmetrical dummy cells was acquired in the frequency range of 10^6 to 0.1 Hz, at the open circuit voltage of 0 V, and the AC modulation amplitude was 10 mV. EIS data analysis was carried out using the Zplot/Zview2 software.

Photovoltaic performances. The photovoltaic properties of DSSCs were measured by recording current–voltage characteristics under illumination with a 1000 W xenon light source (Oriel, 91193) that was focused to give 100 mW cm^{-2} (one sun at AM 1.5G). The light intensity was adjusted with a Si solar cell that was doubled-checked with an NREL calibrated Si solar cell (PV Measurement Inc.). The applied potential and measured cell current were measured using a Keithley model 2400 digital source meter. This process was fully automated using Wavemetrics software. The measurement settling time between applying a voltage and measuring a current for the current–voltage characterization of DSSCs was fixed at 40 ms.

3. Results and discussion

Edge-carboxylated graphene nanoplatelets (ECGnPs) were prepared by a literature procedure[26] (Scheme 1 and the experimental details are described in the ESI†). For comparison, graphene oxide (GO) was also prepared by a modified Hummers' method[27] and it was subsequently reduced using hydrazine to produce rGO (Fig. S1 and see experimental details in the ESI†).[28] The structural differences between ECGnPs and rGO lie in the type and location of the oxygenated groups (Fig. S1†). In particular, ECGnPs have mostly carboxylic acids at the edges of the graphene nanoplatelets (GnPs).[26] On the other hand, rGO has different remnant oxygenated groups (epoxy, hydroxyl, carbonyl, carboxylic acid, *etc.*) at both the edges and the basal plane even after chemical reduction (see Fig. S1†).

The differences in chemical natures could be identified by spectroscopic analyses such as FT-IR (Fig. 1a), XPS (Fig. 1b), and Raman spectroscopy (Fig. 1c). The FT-IR spectrum of ECGnPs

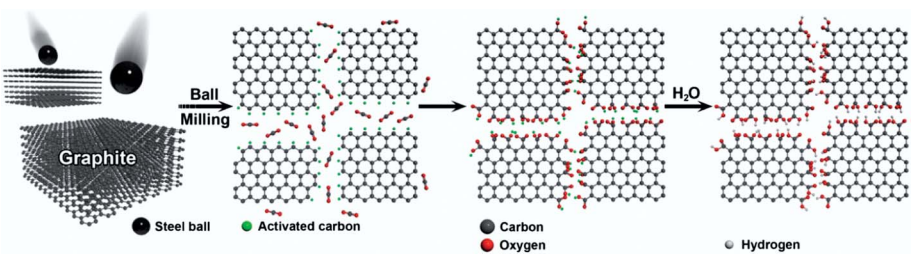

Scheme 1 A schematic representation of the synthesis of edge-carboxylated graphene nanoplatelets (ECGnP) *via* solid-state dry ball-milling graphite in the presence of carbon dioxide.

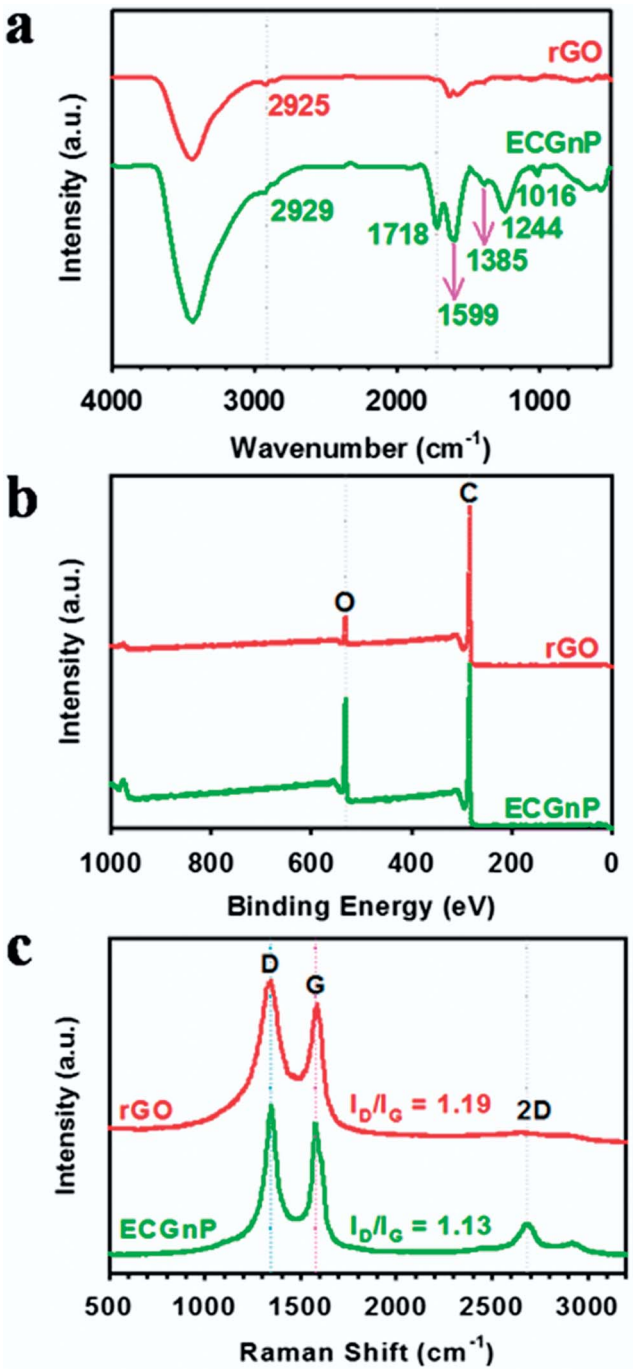

Fig. 1 (a) FT-IR (pellet) spectra; (b) X-ray photoelectron survey spectra; and (c) Raman spectra.

evidently shows strong C=O and C–O stretching peaks from carboxylic acid at 1718 and 1244 cm^{-1}, respectively, while that of rGO shows a weak C=C band at around 1630 cm^{-1} (Fig. 1a). The presence of carboxylic acid in ECGnPs could be further evidenced by XPS measurements. ECGnPs display a relatively pronounced O 1s peak at 532 eV compared with rGO (Fig. 1b), further supporting the oxygen-rich nature of ECGnPs. The high-resolution XPS surveys of C 1s and O 1s are presented in Fig. S2,† showing the similar bond characteristics. Raman spectra of ECGnPs and rGO exhibit similar D-band to G-band (I_D/I_G) ratios of 1.13 and 1.19, respectively, suggesting that significant size reduction has occurred in ECGnPs.

Furthermore, the structural characteristics were studied by microscopic observations (Fig. 2). Obviously, scanning electron microscopy (SEM) images show that EFGnP has a much smaller grain size (<1 μm, Fig. 2a) than rGO (Fig. 2b). SEM images and element mappings (Fig. S3 and S4†) indicate that ECGnPs have a much higher oxygen content, which is consistent with FT-IR and XPS data. On the basis of transmission electron microscopy (TEM) images (Fig. 2c and d) and their selected area electron diffraction (SAED) patterns (insets, Fig. 2c and d), ECGnPs were assumed to have better crystallinity than rGO, due to clearer stripes (arrows) and stronger SAED intensity. Overall, ECGnPs could be produced by a simple one-pot, eco-friendly process and its basal area could also be preserved for better electrical conductivity and oxygen-rich nature at the edges for higher charge polarization (*vide infra*).[26] Hence, ECGnPs are expected to be an advantageous material over the conventional rGO.

Due to the large number of edge-carboxylic acids, the resultant ECGnPs are readily dispersible in many common organic solvents including dimethylsulfoxide (DMSO), *N*,*N*-dimethylformamide (DMF), *N*,*N*-dimethylacetamide (DMAc), *N*-methyl-2-pyrrolidone (NMP) and alcohols, thus they could be deposited on FTO/glass substrates by using an e-spray technique (Fig. S5a†). The transmittance of ECGnP and rGO deposited on FTO/glass substrates by using an e-spray method is shown in Fig. S5b.† While the bare FTO shows a smooth surface (Fig. S6a†), SEM images of FTO surfaces covered with ECGnPs (Fig. S6b†) and rGO (Fig. S6c†) are rough, increasing the surface area thereby improving the electrocatalytic activity. ECGnPs are relatively more uniformly coated on the surface of FTO than rGO. Prior to the sample electrodes used as CEs in DSSCs, the electrocatalytic activities of the ECGnP deposited on FTO for the $Co(bpy)_3^{2+/3+}$ redox couple were systematically examined with cyclic voltammetry (CV) and EIS. Here we also used a PEDOT:PSS/FTO electrode as another reference electrode for comparison, whose transmittance was optimized to about 73% at 550 nm (experimental details are described in the ESI, and see Fig. S7 and S8†). The intrinsic catalytic properties of the sample electrodes were experimentally evaluated using the parameter of R_{CT} at the CE/electrolyte interface, which could be measured by EIS using a symmetrical dummy cell (Fig. 3a).[31] The R_{CT} at the CE/electrolyte interface is a very useful parameter for the evaluation of electrocatalytic activity of the given cathode materials in DSSCs.[31–33] As described in eqn (1), the exchange current density (J_0) varies inversely with R_{CT}, where R is the ideal gas constant, T is the absolute temperature, n is the number of electrons, and F is the Faraday constant.

$$J_0 = \frac{RT}{nFR_{CT}} \quad (1)$$

The Nyquist plots obtained from the symmetrical dummy cells are given in Fig. 3b. The EIS parameters were calculated from the semicircles appeared at the first high-frequency domain using an equivalent circuit (EC, Fig. 3c) and are

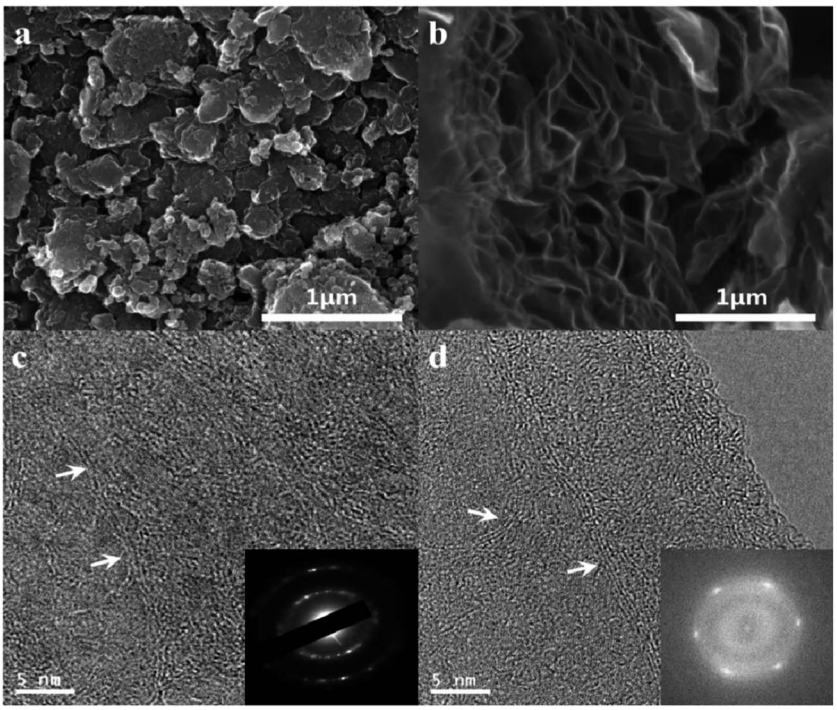

Fig. 2 SEM images: (a) ECGnPs and (b) rGO. Scale bars are 1 μm. TEM images: (c) ECGnPs and (d) rGO.

summarized in Table 1, and see also ESI† for an extended discussion. The ECGnP-CE displayed the EIS parameters, R_S = 1.20 Ω cm^2, R_{CT} = 0.87 Ω cm^2, $1/B = 1.60 \times 10^{-4}$ Ss$^{\beta}$, and β = 0.79. On the other hand, for the rGO-, Pt-, and PEDOT:PSS-CEs, the R_{CT} values were 1.21, 2.19, and 2.63 Ω cm^2, respectively. The R_{CT} of the ECGnP-CE was lower than those of the rGO-, Pt- and PEDOT:PSS-CEs, and the constant phase element (CPE) parameter,[31–33] B, was in proportion to the R_{CT}, which suggested

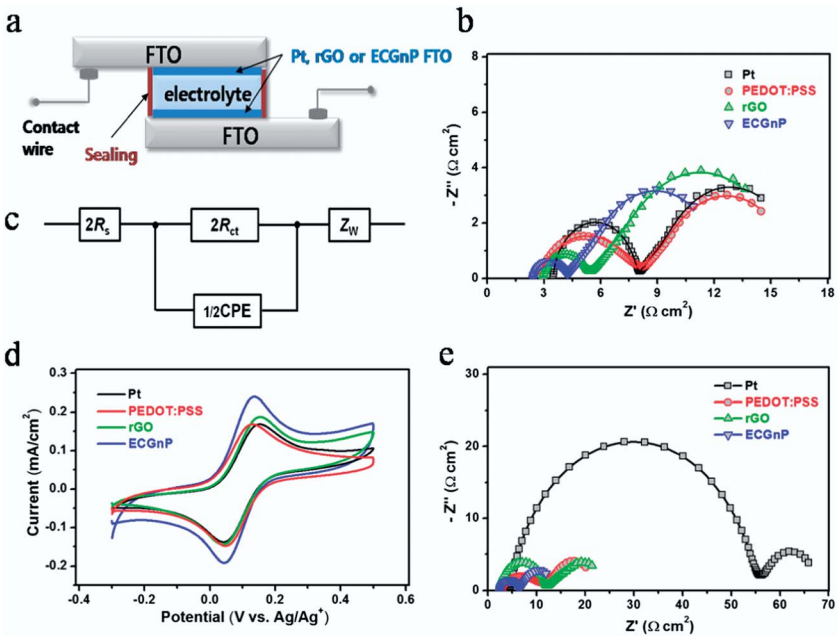

Fig. 3 (a) Typical structure of a symmetrical dummy cell with two identical electrodes; (b) Nyquist plots measured at 0 V from 10^6 Hz to 0.1 Hz on the symmetrical dummy cells; (c) equivalent circuit diagram for fitting the EIS data; (d) cyclic voltammograms obtained at a scan rate of 10 mV s^{-1} for the oxidation and reduction of the $Co(bpy)_3^{2+/3+}$ redox couple using the sample electrodes as the working electrodes, a Pt wire as the CE, Ag/Ag$^+$ as the reference electrode, and 0.1 M $LiClO_4$ as the supporting electrolyte; (e) Nyquist plots of the same dummy cells after a 100 cycle potential *e.g.*, 100 × CV scans (from 0 V → 1 V → −1 V → 0 V at a scan rate of 50 mV s^{-1}).

Table 1 EIS parameters of the sample electrodes in the symmetrical dummy cells

CE	R_S	R_{CT}	CPE:1/B (Ss^{β})	CPE:β	J_0 (mA cm^{-2})
Pt	1.73	2.19	2.72×10^{-5}	0.94	11.7
PEDOT:PSS	1.31	2.63	2.53×10^{-4}	0.66	9.77
rGO	1.44	1.21	1.24×10^{-4}	0.79	21.2
ECGnP	1.20	0.87	1.60×10^{-4}	0.79	29.5

that the electrocatalytic activity was closely related to the R_{CT}. The corresponding J_0 values, calculated from eqn (1), were 29.5 mA cm^{-2} (ECGnPs), 21.2 mA cm^{-2} (rGO), 11.7 mA cm^{-2} (Pt), and 9.77 mA cm^{-2} (PEDOT:PSS) in that order (Table 1). Since the ECGnPs have the lowest R_{CT}, they are expected to show a high FF and PCE in the operation of the DSSCs. Compared to the rGO (Fig. S3 and S4†), the high catalytic activity of ECGnPs could be attributed to their high oxygen-containing polar functional groups (carboxylic acids), which have better charge polarization, and edge-selective functionalization of the GnPs could preserve the conductive graphitic basal plane for better charge transport. Furthermore, the curve fitting of the second semicircles from the Nyquist plots to Z_W with an EC allows the determination of the $Co(bpy)_3^{3+}$ diffusion coefficients (eqn (2)), which were found to be 7.55×10^{-6}, 7.54×10^{-6}, 7.31×10^{-6} and 6.59×10^{-6} cm^2 s^{-1} for the ECGnPs, rGO, Pt, and PEDOT:PSS dummy cells, respectively. The mass transfer of $Co(bpy)_3^{3+}$ in the ECGnP, rGO and Pt is slightly higher than that of the PEDOT:PSS dummy cell. Considering the distance between two electrodes in dummy cells, these values are roughly comparable to the value $D = 9.1 \times 10^{-6}$ cm^2 s^{-1} reported by Feldt *et al.*,[24] using CV on a microelectrode in a similar electrolyte solution.

To support the above-mentioned EIS data, we then investigated the catalytic activities of sample electrodes for the $Co(bpy)_3^{2+/3+}$ redox couple using CV with a typical three-electrode cell, and we used an electrolyte with a concentration lower than the typical concentration used in DSSCs by 100 times. CV curves obtained from the different electrodes show a similar curve shape with pair redox peaks at similar peak positions (Fig. 3d). However, the remarkably high anodic and cathodic peak currents observed for ECGnPs compared with the Pt, PEDOT:PSS and rGO electrodes suggest high electrocatalytic activity for the reduction of $Co(bpy)_3^{3+}$ ions, which could be attributable to the lower R_{CT} at the ECGnP/electrolyte interface as observed in the EIS data. Furthermore, deprotonated oxygen-rich ECGnPs in acetonitrile solution exhibit relatively higher charge polarization than rGO, which might be due to better affinity with the positively charged Co-complex redox couple, resulting in high electrocatalytic performance.

More importantly, electrochemical stability was evaluated with freshly assembled dummy cells. After CV cycles at room temperature, the dummy cells were measured by EIS measurements, and their Nyquist plots are shown in Fig. 3e. The R_{CT} of the ECGnPs was marginally increased to 1.87 Ω cm^2. On the other hand, the R_{CT}s for the PEDOT:PSS, rGO and Pt were increased to 3.92, 4.54 and 25.2 Ω cm^2. Thus, the ECGnPs exhibited a better electrochemical stability than the other electrodes in the $Co(bpy)_3^{2+/3+}$ medium. Moreover, there was no noticeable change in the low frequency region, which indicates that the Co-complex is stable, even with external severe cycling potentials.

The electrocatalytic activities of the sample electrodes as the CEs in the actual devices were evaluated in $Co(bpy)_3$-mediated solar cells with an organic sensitizer (JK-303, Fig. S9a†)[29] and a multi-functional coadsorbent of HC-A (SGT-301, Fig. S9b†).[30] Fig. 4a shows the current–voltage characteristics with the numerical data summarized in Table 2. As can be seen, the Pt-based DSSC exhibited a short circuit current (J_{sc}) of 13.69 mA cm^{-2}, a V_{oc} of 886 mV, a FF of 71.6%, and a PCE of 8.67%. The DSSC with PEDOT:PSS-CE showed photovoltaic performance of a J_{sc} of 13.68 mA cm^{-2}, a V_{oc} of 877 mV, a FF of 68.7%, and a PCE of 8.25%, respectively. The DSSC with the rGO-CE showed an even higher J_{sc} of 13.88 mA cm^{-2}, a V_{oc} of 884 mV, a FF of 72.9%, and a PCE of 8.94%. On the other hand, J_{sc}, V_{oc}, FF, and PCE for the DSSC

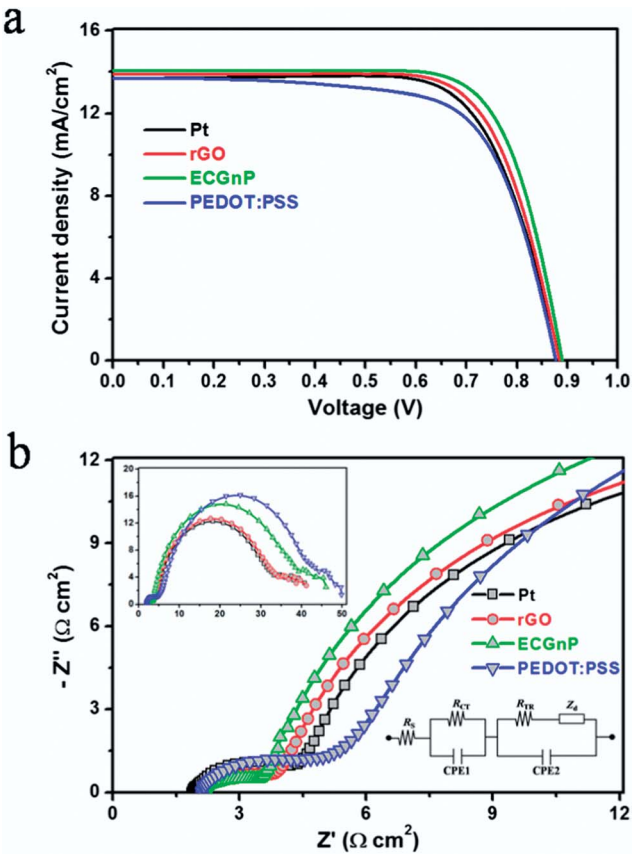

Fig. 4 (a) Current–voltage characteristics of the DSSCs with different CEs under one sun illumination (AM 1.5G). The TiO_2 film thickness is 8.5 (5.5 + 3) μm. All cells were tested with a metal shadow mask having an aperture area of 0.16 cm^2 but without consideration of masking the sides of the DSSCs.[34] (b) Nyquist plots at the high-frequency region of the same DSSCs at a forward bias of −0.8 V under dark conditions. The insets are Nyquist plots (top left) of the full-frequency range and an equivalent circuit (bottom right), respectively.

Table 2 Photovoltaic performance of the DSSCs based on the Pt-, rGO-, PEDOT:PSS- and ECGnP-CEs under one sun illumination (AM 1.5G) (mean of three DSSCs)

CE	J_{sc} (mA cm^{-2})	V_{oc} (mV)	FF (%)	PCE (%)
Pt	13.69 ± 0.03	886 ± 1	71.6 ± 0.4	8.67 ± 0.08
PEDOT:PSS	13.68 ± 0.25	877 ± 5	68.7 ± 1.1	8.25 ± 0.02
rGO	13.88 ± 0.04	884 ± 2	72.9 ± 0.5	8.97 ± 0.10
ECGnP	14.07 ± 0.16	889 ± 1	74.4 ± 0.9	9.31 ± 0.03

with the ECGnPs as a CE were 14.07 mA cm^{-2}, 889 mV, 74.4%, and 9.31%, respectively, whose values were much better than the corresponding rGO- and Pt-CEs. Therefore, it is now obvious that the ECGnP-CE has a higher electrocatalytic activity than rGO-, Pt-, and PEDOT:PSS-CEs stemming from its lower R_{CT}.

To further understand the improved performance in the DSSC based on the ECGnP-CE, the above-mentioned DSSCs were analysed by EIS (Fig. 4b). From the first semicircles, the R_{CT} of the ECGnP-CE (1.62 Ω cm^2) was relatively lower than those of the rGO-CE (1.93 Ω cm^2), Pt-CE (2.61 Ω cm^2), and PEDOT:PSS-CE (3.39 Ω cm^2). The lower R_{CT} at the CE/electrolyte interface would imply a greater FF and J_{sc}, which increase the PCE in DSSCs operation. Moreover, the R_{CT} values were in good accordance with the current–voltage characteristics of DSSCs (FF and J_{sc}, Fig. 4a and Table 2). Furthermore, the efficiencies of the DSSCs with ECGnP-, rGO- and PEDOT:PSS-CEs were moderately decreased without much variation in J_{sc}, FF and V_{oc} in the dark storage at room temperature, whereas that of the DSSC with Pt-CE remarkably decreased due to an decrease in the FF and J_{sc} values (Fig. S10†).

Besides the R_{CT} at the CE/electrolyte interface, the mass transport of the redox couple in the bulk electrolyte solution is one of the main parameters for the efficiency of a DSSC.[31,35] The effect of mass transport of the $Co(bpy)_3^{2+/3+}$ redox couple in complete DSSCs with different CEs was investigated by monitoring photocurrent transients using a multi-step on/off modulation of the mass transfer limitation (Fig. 5).[2,24] As can be seen, the ratio of the initial peak current to the steady state current in the photocurrent transients slightly decreased in the order of PEDOT:PSS- > Pt- > rGO- > ECGnP-DSSCs, indicating that the retarded mass transport can also lead to losses in the photocurrents in the DSSC performances (Fig. 4a). DSSCs based on the Co-complexe redox couples typically suffer a major limitation in terms of slow diffusion of those couples through the pore size of the TiO_2 film.[35] Considering that the DSSCs were fabricated under similar conditions, however, the difference mass transport observed might be governed by the R_{CT} at the interface between the electrolyte and CE. On the basis of the results mentioned above, we can conclude that the improved cell efficiency for the DSSC with ECGnP-CE can be explained by the synergistic effects with the lower R_{CT} and relatively higher mass transport in the bulk electrolyte solution than those of the Pt, PEDOT:PSS, and rGO counterparts.

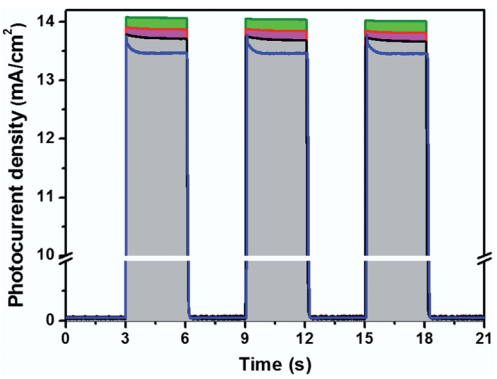

Fig. 5 Photocurrent transient dynamics at simulated full AM 1.5G sunlight: black line: Pt, red line: rGO, green line: ECGnP, and blue line: PEDOT:PSS.

4. Conclusion

In the present study, ECGnPs were prepared by the simple, efficient and eco-friendly dry ball-milling of graphite and evaluated as oxygen-rich metal-free cathodes for the reduction of $Co(bpy)_3^{3+}$ in DSSCs. CV and EIS measurements showed that the ECGnP electrode has greater apparent catalytic activity than Pt, rGO and PEDOT:PSS electrodes, as measured by current density and charge transfer resistant (R_{CT}) at the CE/electrolyte interface, which accounts for its lower R_{CT} in DSSCs. The R_{CT} of the ECGnP-CE decreased to 0.87 Ω cm^2, which is much lower than those of the Pt- (2.19 Ω cm^2), PEDOT:PSS- (2.63 Ω cm^2), and rGO-CE (1.21 Ω cm^2). More importantly, the ECGnP-CE showed better electrochemical stability under prolonged cycling potential than those of its Pt, rGO and PEDOT:PSS counterparts. The DSSC based on the ECGnP-CE displayed a higher FF, a J_{sc} and a PCE (74.4%, 14.07 mA cm^{-2}, 9.31%) than those of the Pt-CE (71.6%, 13.69 mA cm^{-2} and 8.67%), PEDOT:PSS-CE (68.7%, 13.68 mA cm^{-2}, 8.25%) and rGO-CE (72.9%, 13.88 mA cm^{-2} and 8.94%), suggesting that ECGnPs could be one of the promising candidates for the metal-free cathode material in organic DSSCs with the Co-complex redox couple.

Acknowledgements

This work was supported by the Converging Research Center Program through the Ministry of Science, ICT and Future Planning (2013K000203) and the National Research Foundation of Korea (NRF) grant funded by the Korea Government (MEST) (NRF-2012-0001174), and the International Science and Business Belt Program through the Ministry of Science, ICT and Future Planning (former Education, Science and Technology) (2012K001573). JBB would like to acknowledge BRL and Mid-Career Researcher program supported by NRF.

References

1 B. O'Regan and M. Grätzel, *Nature*, 1991, **353**, 737.
2 A. Yella, H. W. Lee, H. N. Tsao, C. Yi, A. K. Chandiran, M. K. Nazeeruddin, E. W. G. Diau, C. Y. Yeh, S. M. Zakeeruddin and M. Grätzel, *Science*, 2011, **334**, 629.

3 (*a*) B. E. Hardin, H. J. Snaith and M. D. McGehee, *Nat. Photonics*, 2012, **6**, 162; (*b*) N. S. Baek, J.-H. Yum, X. Zhang, H. K. Kim, M. K. Nazeeruddin and M. Grätzel, *Energy Environ. Sci.*, 2009, **2**, 1082.

4 (*a*) T. O. Wehling, K. S. Novoselov, S. V. Morozov, E. E. Vdovin, M. I. Katsnelson, A. K. Geim and A. I. Lichtenstein, *Nano Lett.*, 2008, **8**, 173; (*b*) S. B. Yang, X. L. Feng, S. Ivanovici and K. Müllen, *Angew. Chem.*, 2010, **122**, 8586; (*c*) S. B. Yang, G. L. Cui, S. P. Pang, Q. Cao, U. Kolb, X. L. Feng, J. Maier and K. Müllen, *ChemSusChem*, 2010, **3**, 236; (*d*) Q. Su, S. P. Pang, V. Alijani, C. Li, X. L. Feng and K. Müllen, *Adv. Mater.*, 2009, **21**, 3191; (*e*) M. D. Stoller, S. J. Park, Y. W. Zhu, J. H. An and R. S. Ruoff, *Nano Lett.*, 2008, **8**, 3498; (*f*) A. Fasolino, J. H. Los and M. I. Katsnelson, *Nat. Mater.*, 2007, **6**, 858; (*g*) A. A. Balandin, S. Ghosh, W. Z. Bao, I. Calizo, D. Teweldebrhan, F. Miao and C. N. Lau, *Nano Lett.*, 2008, **8**, 902.

5 (*a*) K. S. Novoselov, A. K. Geim, S. V. Morozov, D. Jiang, Y. Zhang, S. V. Dubonos, I. V. Gigorieva and A. Firsov, *Science*, 2004, **306**, 666; (*b*) Y. Zhang, Y.-W. Tan, H. L. Stormer and P. Kim, *Nature*, 2005, **438**, 201.

6 F. Varchon, R. Feng, J. Hass, X. Li, B. N. Nguyen, C. N. Aud, P. Mallet, J. Y. Veuillen, C. Berger, E. H. Conrad and L. Magaud, *Phys. Rev. Lett.*, 2007, **99**, 126805.

7 (*a*) K. S. Kim, Y. Zhao, H. Jang, S. Y. Lee, J. M. Kim, K. S. Kim, J.-H. Ahn, P. Kim, J.-Y. Choi and B. H. Hong, *Nature*, 2009, **457**, 706; (*b*) X. Li, W. Cai, J. An, S. Kim, J. Nah, D. Yang, R. Piner, A. Velamakanni, I. Jung, E. Tutuc, S. K. Banerjee, L. Colombo and R. S. Ruoff, *Science*, 2009, **324**, 1312.

8 (*a*) D. Li, M. B. Muller, S. Gilje, R. B. Kaner and G. G. Wallace, *Nat. Nanotechnol.*, 2008, **3**, 101; (*b*) X. Gao, J. Jang and S. Nagase, *J. Phys. Chem. C*, 2009, **114**, 832.

9 S. M. Feldt, G. Wang, G. Boschloo and A. Hagfeldt, *J. Phys. Chem. C*, 2011, **115**, 21500.

10 R. Jia, J. Chen, J. Zhao, J. Zhang, C. Song, L. Li and Z. Zhu, *J. Mater. Chem.*, 2010, **20**, 10829.

11 (*a*) Z. Yang, T. Chen, R. He, G. Guan, H. Li, L. Qiu and H. Peng, *Adv. Mater.*, 2011, **23**, 5436; (*b*) H. Han, H. Kim, D. Y. Kim, S. M. Jo and S. Y. Jang, *ACS Nano*, 2010, **4**, 3503; (*c*) J. E. Trancik, S. C. Barton and J. Hone, *Nano Lett.*, 2008, **8**, 982.

12 (*a*) W. Hong, Y. Xu, G. Lu, C. Li and G. Shi, *Electrochem. Commun.*, 2008, **10**, 1555; (*b*) H. Choi, H. Kim, S. Hwang, Y. Han and M. Jeon, *J. Mater. Chem.*, 2011, **21**, 7548; (*c*) Y. Xu, H. Bai, G. Lu, C. Li and G. Shi, *J. Am. Chem. Soc.*, 2008, **130**, 5856; (*d*) L. Kavan, J.-H. Yum and M. Grätzel, *ACS Nano*, 2011, **5**, 165; (*e*) L. Kavan, J.-H. Yum and M. Grätzel, *Nano Lett.*, 2011, **11**, 5501; (*f*) I.-Y. Jeon, H.-J. Choi, M. J. Ju, I. T. Choi, K. Lim, J. Ko, H. K. Kim, J. C. Kim, J.-J. Lee, D. Shin, S.-M. Jung, J.-M. Seo, M.-J. Kim, N. Park, L. Dai and J.-B. Baek, *Sci. Rep.*, 2013, DOI: 10.1038/srep02260; (*g*) M. He, J. Jung, F. Qiu and Z. Lin, *J. Mater. Chem.*, 2012, **22**, 24254; (*h*) J. Wang, X. Xin and Z. Lin, *Nanoscale*, 2011, **3**, 3040; (*i*) D. Zhang, X. Li, H. Li, S. Chen, Z. Sun, X. Yin and S. Huang, *Carbon*, 2011, **49**, 5382.

13 (*a*) L. Kavan, J.-H. Yum and M. Grätzel, *ACS Appl. Mater. Interfaces*, 2012, **4**, 6999; (*b*) S. W. Kwon, T. Y. Kim, Y. Kim, M. Byun, Z. Lin, K. S. Suh, D. H. Yoon and W. S. Yang, *Soft Matter*, 2011, **7**, 6811; (*c*) G. Zhu, L. Pan, T. Lu, T. Xu and Z. Sun, *J. Mater. Chem.*, 2011, **21**, 14869.

14 (*a*) G. R. Li, J. Song, G. L. Pan and X. P. Gao, *Energy Environ. Sci.*, 2011, **4**, 1680; (*b*) M. Wu, X. Lin, A. Hagfeldt and T. Ma, *Angew. Chem., Int. Ed.*, 2011, **50**, 3520; (*c*) M. Wang, A. M. Anghel, B. Marsan, N.-L. Cevey Ha, N. Pootrakulchote, S. M. Zakeeruddin and M. Grätzel, *J. Am. Chem. Soc.*, 2009, **131**, 159769; (*d*) H. Sun, D. Qin, S. Huang, X. Guo, D. Li, Y. Luo and Q. Meng, *Energy Environ. Sci.*, 2011, **4**, 2630; (*e*) G. R. Li, F. Wang, Q. W. Jiang, X. P. Gao and P. W. Shen, *Angew. Chem., Int. Ed.*, 2010, **49**, 3653; (*f*) X. Xin, M. He, W. Han and Z. Lin, *Angew. Chem., Int. Ed.*, 2011, **50**, 11739.

15 (*a*) S. Ahmad, J.-H. Yum, Z. X. Xi, M. Grätzel, H.-J. Butt and M. K. Nazeeruddin, *J. Mater. Chem.*, 2010, **20**, 1654; (*b*) Q. Tai, B. Chen, F. Guo, S. Xu, H. Hu, B. Sebo and X.-Z. Zhao, *ACS Nano*, 2011, **5**, 3795; (*c*) H. Wang, Q. Feng, F. Gong, Y. Li, G. Zhou and Z.-S. Wang, *J. Mater. Chem. A*, 2013, **1**, 97.

16 D. S. Yu, E. Nagelli, F. Du and L. M. Dai, *J. Phys. Lett.*, 2010, **1**, 2165.

17 J. D. Roy-Mayhew, D. J. Bozym, C. Punckt and I. A. Aksay, *ACS Nano*, 2010, **10**, 6203.

18 M. J. Ju, J. C. Kim, H.-J. Choi, I. T. Choi, S. G. Kim, K. Lim, J. Ko, J.-J. Lee, I.-Y. Jeon, J.-B. Baek and H. K. Kim, *ACS Nano*, 2013, **7**, 5243.

19 M. Wang, N. Chamberland, L. Breau, J.-E. Moser, R. Humphry-Baker, B. Marsan, S. M. Zakeeruddin and M. Grätzel, *Nat. Chem.*, 2010, **2**, 385.

20 (*a*) S. Caramori, J. Husson, M. Beley, C. A. Bignozzi, R. Argazzi and P. C. Gros, *Chem. – Eur. J.*, 2010, **16**, 2611; (*b*) H. Wang, P. G. Nicholson, L. Peter, S. M. Zakeeruddin and M. Grätzel, *J. Phys. Chem. C*, 2010, **114**, 14300; (*c*) T. Daeneke, T.-H. Kwon, A. B. Holmes, N. W. Duffy, U. Bach and L. Spiccia, *Nat. Chem.*, 2011, **3**, 211; (*d*) Y. Bai, Q. Yu, N. Cai, Y. Wang, M. Zhang and P. Wang, *Chem. Commun.*, 2011, **47**, 4376.

21 (*a*) D. Li, H. Li, Y. Luo, K. Li, Q. Meng, M. Armand and L. Chen, *Adv. Funct. Mater.*, 2010, **20**, 3358; (*b*) H. Tian, X. Jiang, Z. Yu, L. Kloo, A. Hagfeldt and L. Sun, *Angew. Chem., Int. Ed.*, 2010, **49**, 7328; (*c*) Z. Zhang, P. Chen, T. N. Murakami, S. M. Zakeeruddin and M. Grätzel, *Adv. Funct. Mater.*, 2008, **18**, 341; (*d*) Y. Liu, J. R. Jennings, M. Parameswaran and Q. Wang, *Energy Environ. Sci.*, 2011, **4**, 564.

22 (*a*) C. Teng, X. Yang, C. Yuan, C. Li, R. Chen, H. Tian, S. Li, A. Hagfeldt and L. Sun, *Org. Lett.*, 2009, **11**, 5542; (*b*) Z. Ning, H. Tian, H. Qin, Q. Zhang, H. Ågren, L. Sun and Y. Fu, *J. Phys. Chem. C*, 2010, **114**, 15184; (*c*) L. Li, X. Yang, J. Zhao, J. Gao, A. Hagfeldt and L. Sun, *J. Mater. Chem.*, 2011, **21**, 5573.

23 (*a*) H. Nusbaumer, S. M. Zakeeruddin, J.-E. Maser and M. Grätzel, *Chem. – Eur. J.*, 2003, **9**, 3756; (*b*) G. Boschloo and A. Hagfeldt, *Acc. Chem. Res.*, 2009, **42**, 1819; (*c*) Y. Bai, J. Zhang, D. Zhou, Y. Wang, M. Zhang and P. Wang, *J. Am.*

Chem. Soc., 2011, **133**, 11442; (*d*) J.-H. Yum, E. Baranoff, F. Kessler, T. Moehl, S. Ahmad, T. Bessho, A. Marchioro, E. Ghadiri, J.-E. Moser, C. Yi, M. K. Nazeeruddin and M. Grätzel, *Nat. Commun.*, 2012, **3**, 631.

24 S. M. Feldt, E. A. Gibson, E. Gabrielsson, L. Sun, G. Boschloo and A. Hagfeldt, *J. Am. Chem. Soc.*, 2010, **132**, 16714.

25 H. N. Tsao, C. Yi, T. Moehl, J.-H. Yum, S. M. Zakeeruddin, M. K. Nazeeruddin and M. Grätzel, *ChemSusChem*, 2011, **4**, 591.

26 I.-Y. Jeon, Y.-R. Shin, G.-J. Sohn, H.-J. Choi, S.-Y. Bae, J. Mahmood, S.-M. Jung, J.-M. Seo, M.-J. Kim, D. W. Chang, L. Dai and J.-B. Baek, *Proc. Natl. Acad. Sci. U. S. A.*, 2012, **109**, 5588.

27 W. S. Hummers and R. E. Offeman, *J. Am. Chem. Soc.*, 1958, **80**, 1339.

28 S. Park and R. S. Ruoff, *Nat. Nanotechnol.*, 2009, **4**, 217.

29 K. Lim, M. J. Ju, J. Na, H. Choi, M. Y. Song, B. Kim, K. Song, E. Kim and J. Ko, *Chem. – Eur. J.*, 2013, **19**, 9442.

30 (*a*) B. J. Song, H. M. Song, I. T. Choi, S. K. Kim, K. D. Seo, M. S. Kang, M. J. Lee, D. W. Cho, M. J. Ju and H. K. Kim, *Chem. – Eur. J.*, 2011, **17**, 11115; (*b*) M. S. Kang, S. H. Kang, S. K. Kim, I. T. Choi, J. H. Ryu, M. J. Ju, D. Cho, J. Y. Lee and H. K. Kim, *Chem. Commun.*, 2012, **48**, 9349; (*c*) S. H. Kang, I. K. Choi, M. S. Kang, Y. K. Eom, M. J. Ju, J. Y. Hong, H. S. Kang and H. K. Kim, *J. Mater. Chem. A*, 2013, **1**, 3977; (*d*) I. T. Choi, M. J. Ju, S. H. Kang, M. S. Kang, B. S. You and H. K. Kim, *J. Mater. Chem. A*, 2013, **1**, 9114.

31 (*a*) A. Hauch and A. Georg, *Electrochim. Acta*, 2001, **46**, 3457; (*b*) X. Fang, T. Ma, G. Guan, M. Akiyama, T. Kida and E. Abe, *J. Electrochem. Soc.*, 1997, **144**, 876.

32 A. Hagfeldt, G. Boschloo, L. Sun, L. Kloo and H. Pettersson, *Chem. Rev.*, 2010, **110**, 6595.

33 (*a*) T. N. Murakami, S. Ito, Q. Wang, M. K. Nazeeruddin, T. Bessho, L. Cesar, P. Liska, R. Humphry-Baker, P. Comte, P. Pechy and M. Grätzel, *J. Electrochem. Soc.*, 2006, **153**, A2255; (*b*) M. Liberatore, F. Decker, L. Burtone, V. Zardetto, T. M. Brown, A. Reale and A. Di Carlo, *J. Appl. Electrochem.*, 2009, **39**, 229; (*c*) G. Wang, W. Xing and S. Zhou, *J. Power Sources*, 2009, **194**, 568.

34 H. J. Snaith, *Energy Environ. Sci.*, 2012, **5**, 6513, *Nat. Photonics*, 2012, **6**, 337.

35 H. N. Tsao, P. Comte, C. Yi and M. Grätzel, *ChemPhysChem*, 2012, **13**, 2976.